Journal of Mathematical Modeling
Vol. 14, No. 1, 2026, pp. 305-313. Research Article

JMM

Manipulability based model predictive control of rehabilitation robot

Ali Pourmomtaz, Behnam Miripour Fard*, Hamed Kouhi

Faculty of Mechanical Engineering, University of Guilan, Rasht, Iran

Email(s): ali77.pourmomtaz@gmail.com, bmf@guilan.ac.ir, hamed.koohi@guilan.ac.ir

Abstract. One challenge with rehabilitation exoskeletons is the potential for reaching singular configurations, reducing efficiency. Additionally, paths generated for an exoskeleton may not always exhibit optimal manipulability and dexterity, unlike healthy humans who perform tasks with maximum manipulability. This paper considers a multi-degree-of-freedom model for the exoskeleton robot, deriving its kinematic and dynamic equations. The robot's kinematic manipulability is formulated based on the Jacobian, and Model Predictive Control (MPC) is employed for control. The novelty lies in incorporating the cost function related to the robot's kinematic manipulability alongside other cost functions within the MPC framework. Dynamic simulations evaluate this approach, showing that the manipulability criterion conflicts with tracking error. This research demonstrates that using the manipulability index as a constraint or part of the cost function in MPC can help prevent the robot from reaching singular points and enhance manipulability and dexterity in hand rehabilitation.

Keywords: Rehabilitation robot, model predictive control, manipulability.
AMS Subject Classification 2010: 34A34, 65L05.

1 Introduction

The rising number of patients with neurological disorders and strokes has increased the need for rehabilitation robots. According to the World Health Organization, 15 million people suffer from strokes annually, boosting demand for effective rehabilitation methods [1]. Rehabilitation robots-such as ORTE, which is a designated name rather than an acronym-support improved patient outcomes through precise motion control and reduced physical burden on therapists [2]. The ORTE is designed to restore mobility to the shoulder and elbow joints, covering the entire workspace and including various rehabilitation exercises. Robots excel at repetitive tasks without fatigue, making rehabilitation easier than traditional

*Corresponding author
Received: 18 March 2025/ Revised: 12 September 2025/ Accepted: 25 October 2025
DOI: 10.22124/jmm.2025.30154.2695

methods [3]. A major challenge in developing these robots is designing efficient controllers to manage joint positions and forces. The goal is to restore the injured limb's movement capability and skill. High-degree-of-freedom exoskeletons often face efficiency issues due to singular points.

Model Predictive Control (MPC) is used in exoskeleton and rehabilitation robot control. A nonlinear MPC with saturated input showed less tracking error compared to fuzzy and PID controllers [4]. In another study, a three-degree-of-freedom upper limb rehabilitation robot compared PID and MPC algorithms, finding PID had a faster response, while MPC performed better against noise [5]. In [6] the authors developed a model predictive controller based on the Laguerre model to ensure system performance while reducing computational complexity. The results showed that the MPC could achieve simultaneous tracking of joint expected trajectory and speed while meeting various constraints, improving patient motion control ability and reducing fatigue.

While some studies (e.g., [7]) have explored the integration of kinematic manipulability into MPC to improve the control and efficiency of robotic arms, this approach has been less frequently applied to rehabilitation robots. The Authors in [8] presented a design optimization of a robotic system for upper limb rehabilitation based on the manipulability ellipsoid method. The study modeled the human-robot system as a closed kinematic chain and identified the optimal position of the robot base with respect to the patient. The optimization aimed to achieve the best alignment of the manipulability ellipsoids, enhancing the efficiency and effectiveness of the rehabilitation process. This work has not implemented MPC.

The current work significantly contributes by examining the incorporation of kinematic manipulability into the cost function of model predictive control. The primary objectives are to prevent the robot from encountering singular points and to improve both the manipulability and agility during upper limb rehabilitation.

The remainder of this article is organized as follows: Section 2 elaborates on the methodologies used, including the robot modeling, control approach, and the employed manipulaility metrics. In Section 3, the simulation results are presented, followed by the conclusion in Section 4.

2 Methods

The shoulder is the most complex joint of the human body due to its high movements, for which some consider 5 degrees of freedom and others 9 degrees of freedom. In this article, a model similar to the ORTE robot is considered for rehabilitation of shoulder movements. The ORTE robot is designed to reproduce elbow and shoulder rehabilitation exercises. In the following, the kinematic and dynamic analysis of the ORTE is shown. Figure 1 shows the robot and the allocated frames based on Denavit-Hartenberg convention. After allocating the frames based on the Denavit-Hartenberg convention, the transformation matrix of the end-effector in the reference frame is obtained as follows:

$$\mathbf{A_1} * \mathbf{A_2} * \mathbf{A_3} = \begin{bmatrix} C_{23}C_1 & -S_{23}C_1 & S_1 & C_1 l_3 C_{23} + C_1 l_2 C_2 \\ C_{23}S_1 & -S_{23}S_1 & -C_1 & S_1 l_3 C_{23} + S_1 l_2 C_2 \\ S_{23} & C_{23} & 0 & l_1 + l_3 S_{23} + l_2 S_2 \\ 0 & 0 & 0 & 1 \end{bmatrix}. \tag{1}$$

In Equation 1, $\mathbf{A_i}$, for $i = 1,2,3$, is the transformation matrix of frame i. Let $C_1 := cos(\theta_1)$, $S_1 := sin(\theta_1)$, $C_{12} := cos(\theta_2 + \theta_3)$, and so on, as shorthand notation. The variables l_1, l_2 and l_3 denote the lengths of the links.

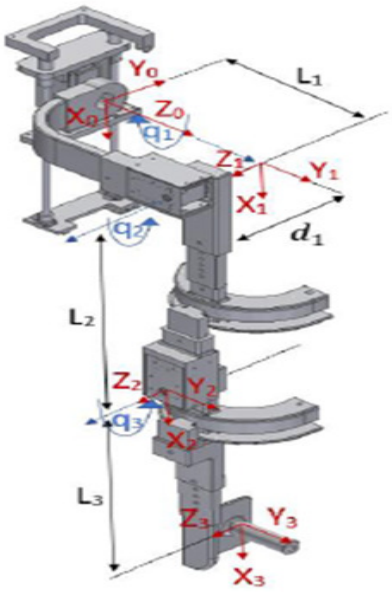

Figure 1: ORTE, exoskeleton designed for rehabilitation purposes [2].

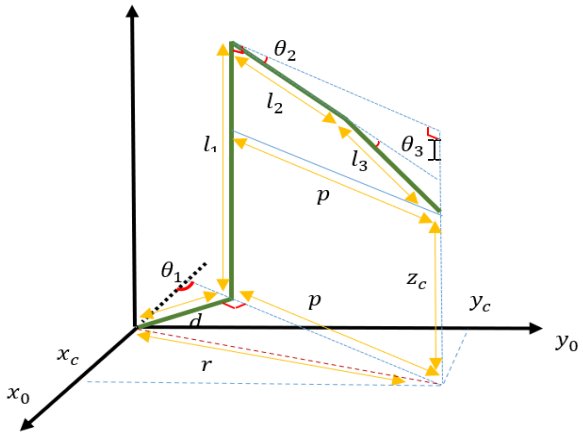

Figure 2: Geometrical view of the robot

A geometric method has been used to solve the inverse kinematics according to Figure 2. In addition, the Jacobian matrix of the robot, which relates joint angular velocities to the end-effector velocities of the robot, is obtained as follows:

$$\mathbf{J} = \begin{bmatrix} -S_1(l_3C_{23} + l_2C_2) & C_1(l_3S_{23} + l_2S_2) & -l_3S_{23}C_1 \\ C_1(l_3C_{23} + l_2C_2) & -S_1(l_3S_{23} + l_2S_2) & -C_1 \\ 0 & l_3C_{23} + l_2C_2 & l_3C_{23} \\ 0 & S_1 & S_1 \\ 0 & -C_1 & -C_1 \\ 1 & 0 & 0 \end{bmatrix}. \tag{2}$$

2.1 Dynamics

The exoskeleton is modeled as a 3-DOF mechanism comprising shoulder flexion/extension (θ_1), shoulder abduction/adduction (θ_2), and elbow flexion/extension (θ_3). All links are assumed rigid and the joints frictionless, matching common biomechanical exoskeleton designs. The Euler-Lagrange method has been used to derive the dynamic equations of the robot. Consider the generalized coordinate as $\mathbf{q} = [\theta_1, \theta_2, \theta_3]^\top$. Define the Lagrangian as

$$L(\mathbf{q}, \dot{\mathbf{q}}) \; = \; T(\mathbf{q}, \dot{\mathbf{q}}) \; - \; V(\mathbf{q}), \tag{3}$$

where T is the total kinetic energy and V the potential energy. The equations of motion follow from

$$\frac{d}{dt}\left(\frac{\partial L}{\partial \dot{q}_i}\right) \; - \; \frac{\partial L}{\partial q_i} = \tau_i, \quad i = 1, 2, 3. \tag{4}$$

the general form of the dynamic equation can be expressed as follows:

$$\mathbf{M}(\mathbf{q})\ddot{\mathbf{q}} + \mathbf{C}(\mathbf{q}, \dot{\mathbf{q}})\dot{\mathbf{q}} + \mathbf{G}(\mathbf{q}) = \boldsymbol{\tau} \tag{5}$$

In Equation (5), $\mathbf{M}(\mathbf{q})$ is the mass and inertia matrix; $\mathbf{C}(\mathbf{q}, \dot{\mathbf{q}})$ is the matrix including Coriolis and centrifugal forces, $\mathbf{G}(\mathbf{q})$ is the gravitational force vector of the robot; and $\boldsymbol{\tau}$ denotes the generalized torque.

We enforce biomechanically feasible joint limits based on [10] as follows:

$$0^\circ \leq \theta_1 \leq 180^\circ, \quad -30^\circ \leq \theta_2 \leq 150^\circ, \quad 0^\circ \leq \theta_3 \leq 135^\circ.$$

Angular velocity and torque bounds are also imposed to reflect safe rehabilitation practice.

2.2 Manipulability-driven MPC

In this paper, we aim to design an MPC system for a rehabilitation robot, incorporating a new term called kinematic manipulability into the MPC cost function and maximizing it. The MPC is a technique that leverages the system model to generate control signals. This involves optimizing a cost function while considering constraints. The control signals are determined over a specified control horizon through an optimization process. The block diagram of the MPC method is shown in Figure 3.

The MPC solves, at each time step, a finite-horizon optimization problem as follows:

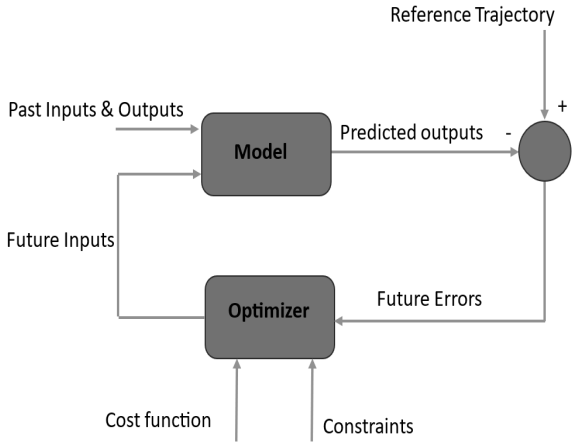

Figure 3: General architecture of MPC method used in the current work.

$$\min_{\{\boldsymbol{\tau}(k)\}} \sum_{k=0}^{N-1} \left\| \mathbf{q}(k) - \mathbf{q}^d(k) \right\|_{W_1}^2 + \|\Delta\boldsymbol{\tau}(k)\|_{W_2}^2 - w_3\, \mu\left(\mathbf{q}(k)\right), \tag{6}$$

subject to the continuous-time dynamics (5), input saturations, and joint limits. Here, $W_1 \in \mathbb{R}^{3\times3}$ penalizes tracking error, $W_2 \in \mathbb{R}^{3\times3}$ penalizes control effort, and $w_3 > 0$ trades off manipulability. By directly embedding the Euler–Lagrange–based model into the prediction, the MPC respects the robot's true dynamics and enforces all safety constraints. In (6), vectors $\mathbf{q}$ and $\mathbf{q}^d$ represent the actual and desired joint configurations, respectively and μ is the kinematic manipulability index will be defined next in this section. A series of constraints are also considered on the input torque range.

In our implementation, we discretize the dynamic model in (5) using a forward Euler integration with sampling time T_s. We define the state vector at instant k as

$$\mathbf{x}(k) = \begin{bmatrix} \mathbf{q}(k) \\ \dot{\mathbf{q}}(k) \end{bmatrix}, \quad \mathbf{x}(k+1) = \mathbf{x}(k) + T_s \left[\dot{\mathbf{q}}(k)\, M^{-1}\left(\mathbf{q}(k)\right) \left(\boldsymbol{\tau}(k) - C(\mathbf{q}(k), \dot{\mathbf{q}}(k))\, \dot{\mathbf{q}}(k) - G(\mathbf{q}(k)) \right) \right].$$

The MPC then optimizes the torque sequence $\{\boldsymbol{\tau}(0), \ldots, \boldsymbol{\tau}(N-1)\}$ by minimizing the above cost over a horizon N, subject to:

- Discrete-time dynamics $\mathbf{x}(k+1) = f\left(\mathbf{x}(k), \boldsymbol{\tau}(k)\right)$ as shown above.
- Joint limits: $\theta_i^{\min} \le \theta_i(k) \le \theta_i^{\max}$, $i = 1,2,3$.
- Torque bounds: $\tau_i^{\min} \le \tau_i(k) \le \tau_i^{\max}$.
- Rate-of-change limits: $\Delta\boldsymbol{\tau}(k) = \boldsymbol{\tau}(k) - \boldsymbol{\tau}(k-1)$, with $\|\Delta\boldsymbol{\tau}(k)\| \le \Delta\tau^{\max}$.

Kinematic manipulability measures a robot's ability to position its end-effector in a specific configuration, reflecting its agility. A robot has higher manipulability if its end-effector can achieve a wider

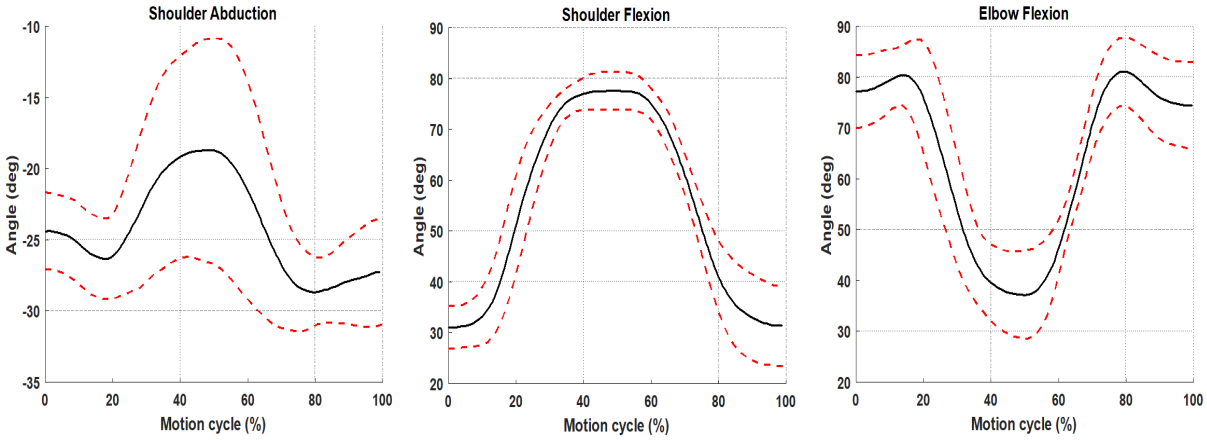

Figure 4: Desired trajectories of shoulder flexion, shoulder abduction and elbow flexion. The black solid lines show the mean and the red dashed lines show the standard deviation ranges.

range of speeds at a given time and configuration. This criterion also indicates how well the robot avoids singular configurations, where manipulability is zero. The mathematical expression for kinematic manipulability is as follows:

$$\mu = \sqrt{\det\left(\mathbf{J}(\mathbf{q})\mathbf{J}(\mathbf{q})^{\top}\right)} \tag{7}$$

In Equation (7), $\mathbf{J}(\mathbf{q})$ is the Jacobian matrix and μ represents the volume element induced by the Jacobian. The ability to generate velocity for the end-effector in different directions can also be represented by an ellipse on a plane or an ellipsoid in space. The major axis of the ellipse indicates the direction in which the end effector can move faster.

3 Results and discussion

Different scenarios can be explored for rehabilitation simulation. In this section, we will present the results for a scenario where the patient moves their hand towards the table and then returns it to the starting position. The desired trajectories for each joint involved in this movement have been derived from experimental motion analysis of human movements, as presented in [9]. These reference trajectories are illustrated in Figure 4. Notably, the significant standard deviation suggests that individuals employ varying pathways for identical movements across different iterations. This observation underscores the diminished relevance of precisely tracking paths during the rehabilitation process. Moreover, it will be demonstrated later in this paper that the proposed method also attributes less importance to exact path tracking.

Figure 5 presents the simulation results depicting joint variations under two scenarios: one accounting for manipulability and the other disregarding it. According to Figure 5, The results indicate that taking manipulability into account does not yield identical tracking of reference trajectories compared to scenarios where manipulability is not considered.

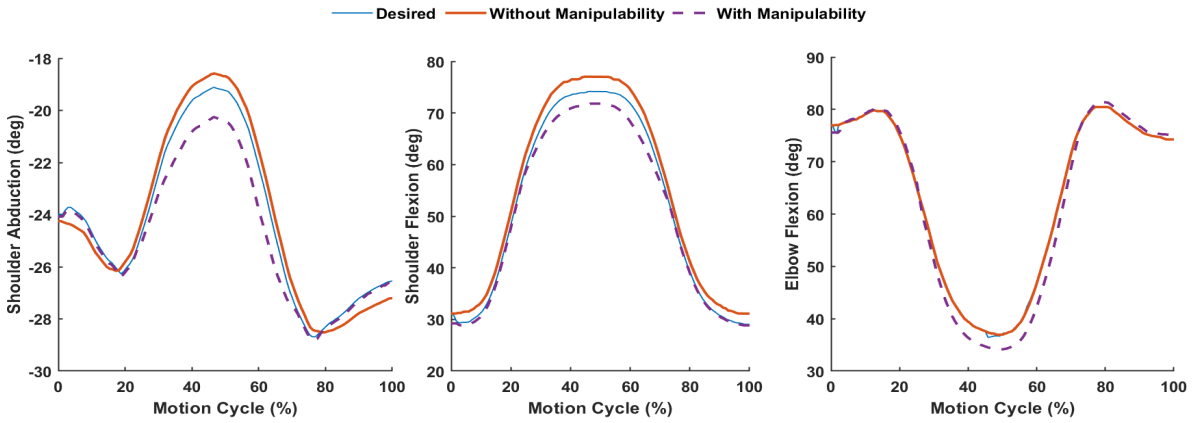

Figure 5: Joint angular trajectories

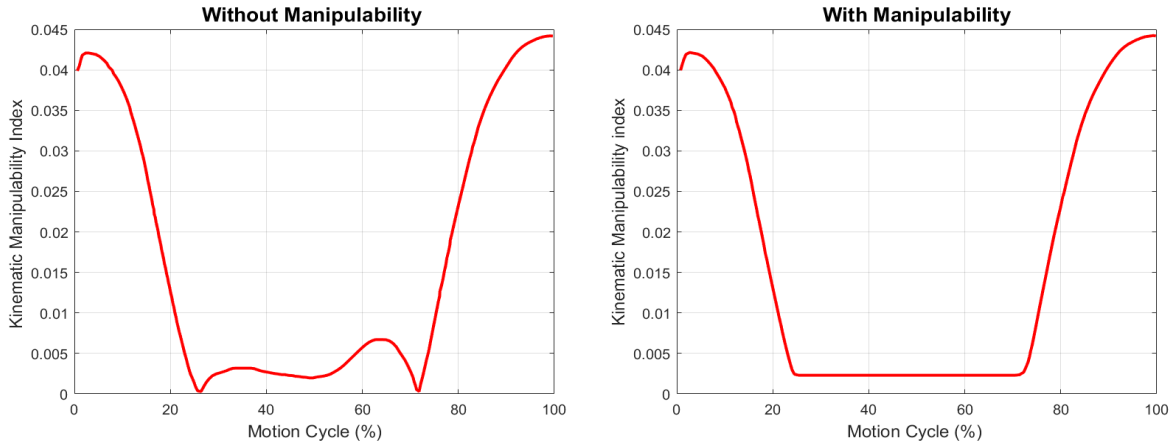

Figure 6: Kinematic manipulability index under two scenarios: without manipulability and with manipulability

Figure 6 illustrates the variations in the manipulability index for two scenarios. It is evident from the figure that, in the absence of manipulability index in the control, the robot reached a singular configuration twice, which is highly undesirable.

Figure 7 shows the joint torques in the two cases. It is clear that due to the kinematic differences in the two scenarios, the joint torques are also different.

The nonlinear MPC is implemented in MATLAB R2020b using the `fmincon` function with the interior-point algorithm. We set solver options as:

$$\texttt{OptimalityTolerance} = 10^{-6}, \quad \texttt{StepTolerance} = 10^{-6}, \quad \texttt{MaxIterations} = 200.$$

At each control step, we warm-start `fmincon` with the previous control sequence. Computations are performed on a ASUS (Intel Core i7-10510U @ 1.8 GHz, 8 GB RAM).

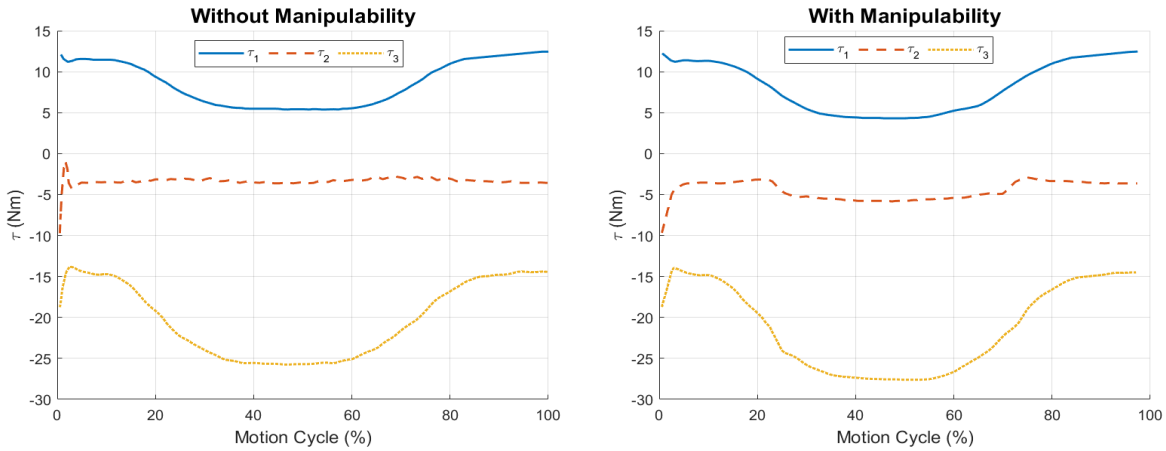

Figure 7: Joint torques under two scenarios: without manipulability and with manipulability. τ_1 represents shoulder flexion, τ_2 signifies shoulder abduction, and τ_3 denotes elbow flexion.

With prediction horizon $N = 20$ and sampling time $T_s = 0.02\,\text{s}$, the average `fmincon` solution time is 20s, and 95% of solves complete under 30s.

4 Conclusion

In this paper, kinematic and dynamic modeling of a rehabilitation robot are performed, and a nonlinear model predictive controller is used for control. For the first time, kinematic manipulability is included in the cost function alongside tracking error and energy consumption. The goal is to minimize tracking error and energy consumption while maximizing manipulability. A simulated rehabilitation scenario showed that adding manipulability to the cost function slightly increased tracking error. Thus, a balance between manipulability, tracking error, and energy consumption is necessary. While this may not be ideal for robotics, it is significant for rehabilitation, where precise path tracking is less critical, and more emphasis can be placed on manipulability. Reaching the target point (e.g., the mouth) remains important and can be achieved by modifying the algorithm. A comprehensive sensitivity analysis of the weighting matrices W_1, W_2, and scalar weight w_3 is recognized as an important extension and will be pursued in future work to further characterize the precision–dexterity trade-off.

Conflicts of interest

The authors declare that there are no conflicts of interest.

References

[1] S.Y. Raza, S.F. Ahmed, A. Ali, K.A. Kadir, M.K. Joyo, S. Khan, Z. Janin, *Model predictive control for upper limb rehabilitation robotic system under noisy condition*, Proc. IEEE 5th Int. Conf. Smart Instrumentation, Measurement and Application (ICSIMA), Nov. 2018, 1–4.

[2] M.A. Destarac, J.G. Montano M. Cardona, E. Gomez, *Orte exoskeleton: Kinematic analysis and dynamic modeling*, Proc. IEEE 38th Central America and Panama Convention (CONCAPAN XXXVIII), 2018.

[3] H.S. Lo, S.Q. Xie, *Exoskeleton robots for upper-limb rehabilitation: State of the art and future prospects,* Med. Eng. Phys. **34** (2012) 261–268.

[4] S.M.T. Zarandi, S.K.H. Sani, M.R.A. Tootoonchi, A.A. Tootoonchi, M.G Farajzadeh, *Design and implementation of a real-time nonlinear model predictive controller for a lower limb exoskeleton with input saturation,* Iran. J. Sci. Technol. Trans. Electr. Eng. **45** (2021) 309–320.

[5] A. Ali, S.F. Ahmed, M.K. Joyo, K. Kushsairy, *MPC-PID comparison for controlling therapeutic upper limb rehabilitation robot under perturbed conditions*, Proc. IEEE 3rd Int. Conf. Eng. Technol. Soc. Sci. (ICETSS), 2017.

[6] Y. Yan, et al., *Trajectory tracking control of wearable upper limb rehabilitation robot based on Laguerre model predictive control,* Robot. Auton. Syst. **179** (2024) 104745.

[7] G.B. Avanzini, A.M. Zanchettin, P. Rocco, *Constrained model predictive control for mobile robotic manipulators*, Robotica **36** (2018) 19–38.

[8] G. Chiriatti, A. Bottiglione, G. Palmieri, *Manipulability optimization of a rehabilitative collaborative robotic system,* Machines **10** (2022) 452.

[9] M.C. Molet, J.L. Prat, *Analysis of arm movements during activities of daily living for the design of an active upper limb exoskeleton for adults with Duchenne,* M.Sc. Thesis, Dept. Mech. Eng., Universidad Politecnica de Catalunya, Barcelona, Spain, 2016.

[10] D.A. Winter, *Biomechanics and Motor Control of Human Movement*, 3rd ed., John Wiley & Sons, Hoboken, NJ, USA, 2009.